# MANG@COAST: A NOVEL SPATIO-TEMPORAL MODELING APPROACH OF MUDDY SHORELINE MOBILITY BASED ON MANGROVE MONITORING

Augusseau P.E.[1,2,3], Proisy C[1,2*], Gardel A.[3], Brunier, G.[3,4], Granjon, L.[3], Maury, T.[3], Mury, A.[2,5], Staquet, A.[1,2,3], Santos V.F.[6], Walcker R.[7], Degenne P.[8], Lo Seen D.[8], Anthony E.J.[9]

1 - AMAP, IRD, Cayenne, French Guiana, France paul-emile.augusseau@ird.fr; christophe.proisy@ird.fr

2 - AMAP, IRD, CIRAD, CNRS, INRAE, Univ. Montpellier, Montpellier, France adrien.staquet@ird.fr

3 - LEEISA, CNRS, Univ. Guyane, Cayenne, French Guiana antoine.gardel@cnrs.fr; ludovic.granjon@cnrs.fr; tanguy.maury@cnrs.fr

4 - BRGM, Cayenne, French Guiana, France; g.brunier@brgm.fr

5 - iSEA, Pessac, France antoine.mury@ird.fr

6 - Instituto de Pesquisas Científicas e Tecnológicas do Estado do Amapá (IEPA), Macapá, Amapá, Brazil valdeniraferreira@gmail.com;

7 - Centre de Recherche sur la Biodiversité et l'Environnement (CRBE), Université de Toulouse, CNRS, IRD, Toulouse INP, Université Toulouse 3 – Paul Sabatier (UT3), Toulouse, France. romain.walcker@univ-tlse3.fr

8 - UMR TETIS, CIRAD, Montpellier, France pascal.degenne@teledetection.fr; danny.lo-seen@teledetection.fr

9 - Aix-Marseille Université, Institut Universitaire de France, CEREGE, Aix en Provence, France. anthony@cerege.fr

*: corresponding author

**Abstract**

Monitoring mangroves could prove invaluable for developing new coastal erosion models. We present a multiscale modeling approach for mangrove shoreline fluctuations observed over 10 years using satellite imagery acquired along the open, dynamic muddy coast of French Guiana. We aimed to gain a better understanding of the complex interactions between ocean waves and mud banks by simulating the processes that lead to both mangrove erosion and expansion. We found that fluctuations in seafront mangroves could be simulated with acceptable accuracy along 200 km of coastline. In the absence of mud banks, seasonal wave forcing resulted in erosion rates reaching 1100 m/y. Our findings indicate that wave energy can be reduced by 90% at all locations when the extent of mud banks exceeds 2000 m in front of the mangroves. Finally, we discuss the potential of this innovative modeling approach for anticipating coastal changes.

**Highlights**

1. MANG@COAST simulates mangrove fluctuations on the muddy French Guiana coast.
2. MANG@COAST is calibrated with satellite observations covering 10 years and a swathe of 200 km.
3. The model quantifies the critical role of mud banks in attenuating waves and protecting mangroves.
4. Mangrove ability to expand is a key process in modeling coastal changes.

**Keywords:** Landscape evolution model; open coast; wave attenuation; remote sensing; Amazon sediments; French Guiana

**Software and/or data availability**

**Name of software:** MANG@COAST
**Developer and contact information**: PROISY Christophe christophe.proisy@ird.fr
**Year first available:** 2024
**Hardware required**: Personal Computer systems running Java (e.g. Windows or Linux PC)
**Software required:** Java 8, command prompt able to run the command “java –jar”
**Availability and cost**: Direct download, free
**Program language:** Ocelet / Java
**Program size**: 77 kb (main software) + 31.1 Mb (software library folder)
**Software license**: CC BY NC SA - https://creativecommons.org/licenses/by-nc-sa/4.0/deed.en
**Access to the code and data**: Download the zip link (from the code button) or make a git clone of the repository from https://github.com/OceletTeam/Mangacoast.

## 1. Introduction

Coastal erosion processes are difficult to mitigate and complex to predict (Foster-Martinez et al. 2020). For muddy coasts, the challenge of predicting the erosion risk is even greater, because muddy coasts are much more dynamic than sandy coasts (Hulskamp et al. 2023). Muddy coasts account for ~14% of the world's ice-free coastlines, 60% of which are located in the tropics (Hulskamp et al. 2023). They are generally characterized by large and low-gradient intertidal and subtidal areas (Mehta 2002; Wang et al. 2002). Wave action is the dominant erosive force on muddy coasts (Anthony et al. 2022; Mehta 2002; Rodriguez and Mehta 2001); waves remobilize and disperse fine-grained sediments over long distances (Anthony et al. 2022; Gratiot and Anthony 2016), whereas on sandy coasts non-cohesive sediments reshape beach profiles (Gao 2019; Wang et al. 2002). Muddy deposits undoubtedly play an important role in attenuating wave energy (Jain and Mehta 2009; Winterwerp et al. 2007). However, field studies quantifying the wave attenuation profile as a function of the extent and elevation of muddy deposits are scarce because of the extreme difficulty in assessing the volume of remobilized sediment (Toorman et al. 2018). This probably explains why modeling studies on the effects of ocean wave forcing on muddy coasts are not as common as those proposed for sandy coasts (Castelle et al. 2022; Robinet et al. 2018; Splinter and Coco 2021; Toimil et al. 2020). Locally, muddy coasts can undergo massive erosion caused by waves, which is sometimes exacerbated by the presence of urban and engineering infrastructures, even when the latter are designed to protect the coast (Anthony and Gratiot 2012; Brunier et al. 2019). According to Reguero et al. (2019), worldwide, wave energy is expected to increase by 0.4% annually. Combined with sea level rise, the impact, in terms of wave run-up and excursion, is likely to be felt over long distances in muddy areas with low elevation gradients (McGranahan et al. 2007). An improved understanding of how wave forcing causes the erosion of muddy coasts will contribute to better coastal management.

Mangrove forests can develop in tidal saline wetlands along tropical and subtropical coastlines, where they are protected from the direct action of the ocean (Blasco et al. 1996; Saenger 2003). Their presence is likely to have a mitigating effect on sea level rise (Ellison 2019), and they act as natural coastal buffers against extreme events (Temmerman et al. 2023). There are several studies aimed at understanding their role in attenuating wave action, particularly following the devastating Indian Ocean tsunami in December 2004 (Mazda et al. 2007; Tanaka et al. 2007).

Mangrove forests can thrive only on open coasts where a continuous and abundant supply of sediment is present (Anthony et al. 2022). However, the mere presence of a large mangrove fringe is not sufficient to stabilize an eroded shoreline (Besset et al. 2019; Gedan et al. 2011). This is evidenced by a 68-year spatial analysis of mangrove shoreline fluctuations along approximately 300 km of coastline in French Guiana (FG), which showed that cross-shore rates of mangrove retreat can reach

500 m per year at deeper, relatively mud-deficient locations (called interbank areas) between large dissipative mud banks (Proisy et al. 2021), which are defined as a hyper-charged mass of coastal mud in which concentrations can exceed 1000 g/L. Mud banks may be mobile alongshore, under the influence of waves and currents, or stationary (Anthony et al. 2022), and the seaward edge of coastal mangroves is sensitive to relatively energetic Atlantic waves and decadal oceanic regional climate trends, depending on the changing morphology induced by the northwest drifting mud banks (Walcker et al. 2015). Thus, a clearer picture of the role of mangroves in mitigating coastal erosion requires the consideration of the characteristics of the muddy shore context with which they are associated.

Further research is required to integrate mangrove studies into attempts to model the vulnerability of open, muddy coasts to wave erosion. The growing accessibility of operational remote sensing techniques, spanning global (Bunting et al. 2022) to local scales (Ghosh et al. 2022), coupled with the vast repository of satellite imagery of mangroves and coasts, presents a promising avenue for modeling alterations in mangrove shorelines.

However, mangrove models have been designed to analyze vegetation development processes, independently of coastal erosion processes. The focus has been on the analysis and prediction of forest stand dynamics (Berger et al. 2008). Tree diameter growth equations, which can be weighted by environmental factors, such as salinity or air temperature, are calibrated for different species and biogeochemical contexts. Recently, an integrative approach was published by Beselly et al. (2023) to couple a hydrodynamic model describing environmental processes (water level, current, sediment availability, and salinity) with an individual-based model that calculates tree growth from the earliest stages of propagule recruitment to simulate mangrove expansion. The model works at a local scale over an area of approximately 2500 m × 500 m on a prograding tidal flat subject to sediment supply. We believe that vegetation-centered models need to be linked to the impacts of climate change on the coast to provide a regional assessment of the adaptive capacity of mangroves to coastal erosion processes, which are likely to be a key process in mangrove mortality everywhere, from the tree or forest stand to the regional scale.

This study presents a novel approach aimed at modeling the impacts of unquantified erosion processes on the open muddy coast of French Guiana (FG), which is considered to be one of the most dynamic in the world (Anthony et al. 2010). To clarify this, we focused on marine erosion at the seaward mangrove edge, which is easily observable from space (Proisy et al. 2021) and is primarily affected by the intensity and variability of wave processes.

Our model, MANG@COAST, was developed based on the Ocelet domain-specific language, which was specifically designed to model spatiotemporal landscape changes using interaction graphs (Degenne and Lo Seen 2016). This allowed us to express flexibly how the key landscape units of mangrove muddy coasts interact. Therefore, we proposed a set of two equations and three parameters

to relate changes in mangrove shorelines (the variables to be explained) to ocean waves attenuated by mud banks of varying shapes, extents, and locations (the explanatory variables). The coefficient values were obtained by minimizing the differences between the observed and simulated mangrove shorelines. After assessing the performance and quality of the model, we analyzed the spatial and seasonal variability of erosion processes induced by typical wave patterns and highlighted the wave attenuation effect of mud banks along the mangrove-rich FG coast. We discuss the implications of our model for a more accurate interpretation of the interactions between waves, mud banks, and mangroves, as well as the capabilities and limitations of MANG@COAST for coastal zone management in French Guiana Furthermore, we present some potential future developments of this adaptable modeling approach.

## 2. Materials and methods

### 2.1. Study area

The study area covers approximately 200 km of the 320 km long FG coast, from Cayenne to the Maroni River estuary at the boundary with Suriname (Fig. 1a). Approximately 80–90% of the FG coastline is covered by mangroves. The physiognomy of this coast is shaped by recurrent hydrodynamic and sedimentary processes (Gensac et al. 2016). The northwest alongshore migration of several mud banks along the FG coast results in space- and time-varying depositional 'bank' phases and erosional 'inter-bank' phases at any location on the coast (Anthony et al. 2010; Froidefond et al. 1988; Toorman et al. 2018).

During interbank phases, mangrove trees are uprooted by the erosion of the muddy substrate on which they grow (Fig. 1b), and mangrove shorelines retreat rapidly. In FG, muddy shorelines of open coasts, with or without mangroves, erode according to several processes observed in the field (Brunier et al. 2019). The main process is the collapse of muddy plastic deposits by waves together with mud liquefaction, which explains the extremely rapid erosion rates observed. Along the inter-bank areas, sand deposits can accumulate on top of the muddy shoreline because of erosion. They eventually form sandy beach ridges, known as 'chenier' beaches (Anthony et al. 2022), where human occupation generally occurs.

Subsequent accretion phases can rebuild muddy deposits that buffer and isolate onshore chenier beaches from the intertidal zone. (Proisy et al. 2021). Mangroves can expand rapidly during bank phases (Fig. 1c) and extensively (Proisy et al. 2009). Additional illustrative information on the hydro-sedimentary context, mangrove forests, and socio-environmental challenges in the FG can be found in Proisy et al. (2022).

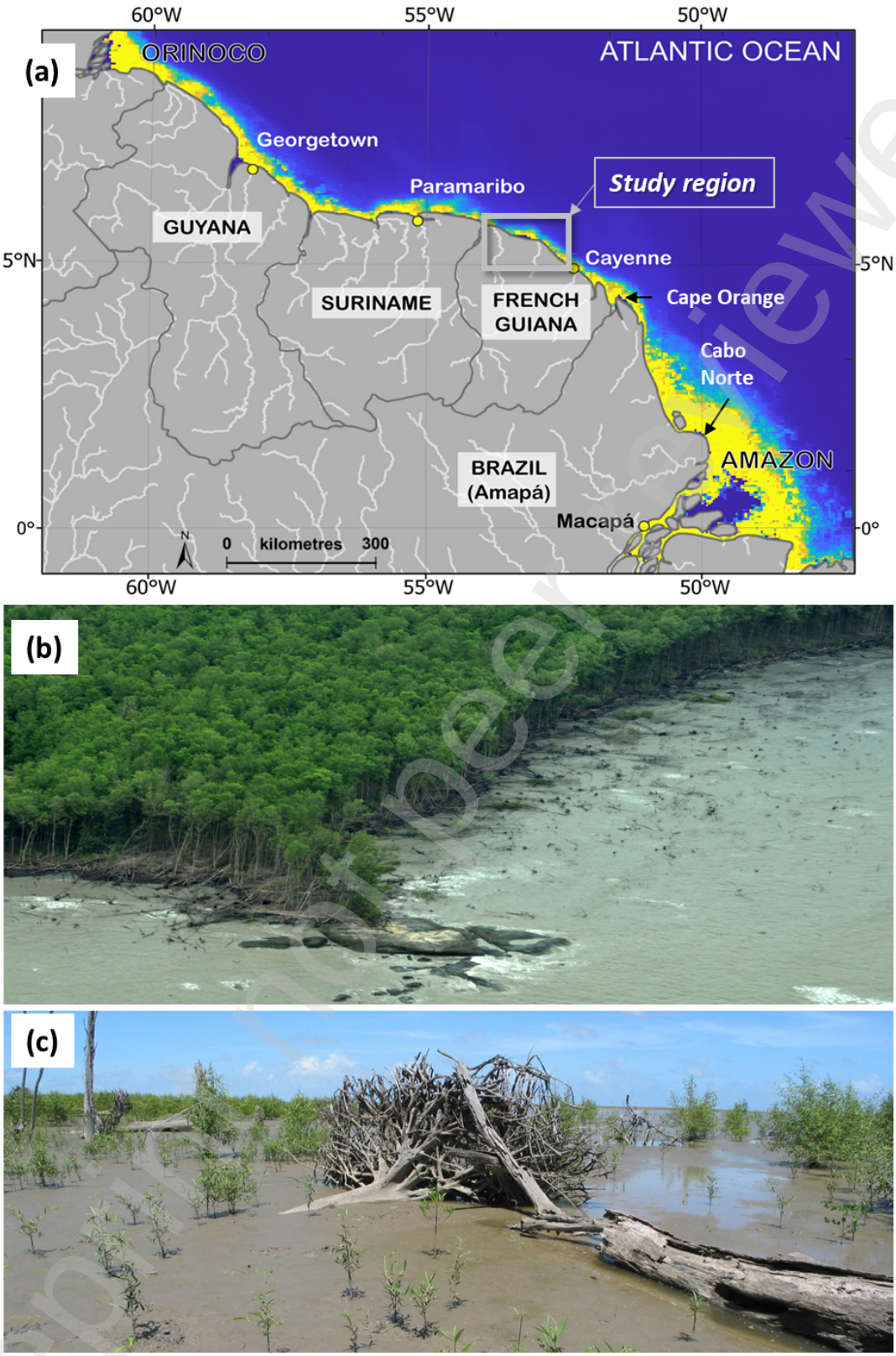


**Fig. 1.** Mangrove-rich French Guiana coast. (a) Regional context, i.e., 1500 km coastline under the influence of mud from the Amazon and the 200-km long study area. Yellow color indicates suspended particulate matter (SPM) mapped from the Marine Copernicus dataset. (b) Mangrove trees are uprooted as a result of mud substrate erosion by waves. (c) Newly consolidated mud banks can lead to mangrove colonization, whereas trees uprooted during the last phase of erosion have not yet fully decomposed.

## 2.2. Landscape evolution modeling with Ocelet

MANG@COAST simulates the changes in mangrove coastlines in response to external forces. Our model can therefore be seen as a landscape evolution model (Tucker and Hancock 2010; Valters 2016), in which the governing processes of coastal change remain too complex and intertwined to envisage the formulation of equations, which requires a numerical solution method to calculate approximate solutions to the observations. To address this numerical challenge, we implemented MANG@COAST under the "Ocelet Modeling Platform" (OMP). Ocelet is a modeling language and environment (Degenne et al. 2009) that allows the simulation of spatial dynamics using interaction graphs with entities as vertices and interaction functions attached to their edges (Degenne and Lo Seen 2016). Entities can be viewed as the actors in this model. They are typically georeferenced and have properties with values that describe the initial and changing states under the influence of interactions. The relationships (or interactions) between the entities were described using mathematical expressions. A scenario (the main model code) was set up to initialize, activate, and control the execution of relations between entities in time and space. Interactions between entities result in changes in their state and (spatial) configuration. Points, lines, polygons, and all data types commonly employed in Geographical Information Systems (GIS), are used to represent entities in Ocelet. This approach is intuitive, as one has to design a dynamic system by describing the interactions between entities that influence the temporal evolution of the entire system. Entities no longer belong to a "GIS layer" and their state results from interactions with other entities through space and time.

Ocelet-based modeling approaches have been successful in various case studies, including agriculture (Jahel et al. 2018), mosquito population dynamics (Tran et al. 2019), or land planning (Russeil et al. 2023). Proisy et al. (2016) made a preliminary attempt to model mangrove shoreline dynamics using the Ocelet Modeling Platform. We improved this preliminary version to take advantage of the availability of new data on mud banks and enhanced spatial resolution of the ocean wave dataset. This is explained in the following sections.

## 2.3. MANG@COAST model

MANG@COAST excludes mangroves developed in estuaries, behind cheniers, and upstream rivers. Only mangroves that developed on the open coast, that is those that could potentially be destroyed by wave action, were considered.

### *2.3.1 Entities and modeling principle*

MANG@COAST, was designed using four entities (Fig. 2):

1 The “ocean” entity deals with the forcing mechanisms induced by ocean waves approaching the mangrove coast. In the preliminary version of the model (Proisy et al. 2016), forcing mechanisms generated by ocean currents were also considered to simulate the northwestward migration of the FG mud banks. Now that the shapes and locations of the mudbanks are available as input data, the present model has been simplified, and ocean current data are no longer required.

2 The “mud bank” entity plays the role of attenuating the wave-induced forcing processes. This corresponds to the area of intertidal mud extending seawards by the 5 m isobath value (water depth), below which wave height attenuation is rarely detected (Abascal Zorrilla et al. 2018).

3 The “mangrove” entity corresponds to the extent of mangroves in French Guiana.

4 The “chenier” entity corresponds to the landward limit of the coastal mangrove areas. Cheniers are commonly isolated by muddy progradation onward and landward, where human occupation generally occurs.

During bank phases, the ‘ocean’ entity interacts (f1) with the seaward boundary of the mud bank (Fig. 2). The impact on each point of the sea-mangrove shoreline, i.e., a spatial feature of the ‘mangrove’ entity, is then calculated from the attenuation (f2) of (f1) provided by the ‘mud bank’ entity. During inter-bank phases, the ‘ocean’ and ‘mangrove’ entities interact directly (f2=0). During the bank phase, the mud bank also interacts with the 'surface area' property of the ‘mangrove’ entity to modulate the mangrove expansion process (f3). The mangrove shoreline at any point on the coastline was recalculated annually, considering the daily effects of the wave forcing signal and the annual northwesterly migration of mud banks.

### *2.3.2 Data*

These four entities were associated with different datasets of different formats and sizes. Their preparation for the operation of MANG@COAST has been a long-term undertaking involving the manipulation and analysis of vast amounts of remotely sensed imagery and marine data in various formats. These datasets are available with the download of MANG@COAST from the Ocelet Modeling Platform and detailed information is given in Appendix A. Datasets describing mud banks, mangroves, and cheniers are processed directly by Ocelet in their native ESRI Shapefile format. These maps can be produced automatically, as shown in Fig. 3.

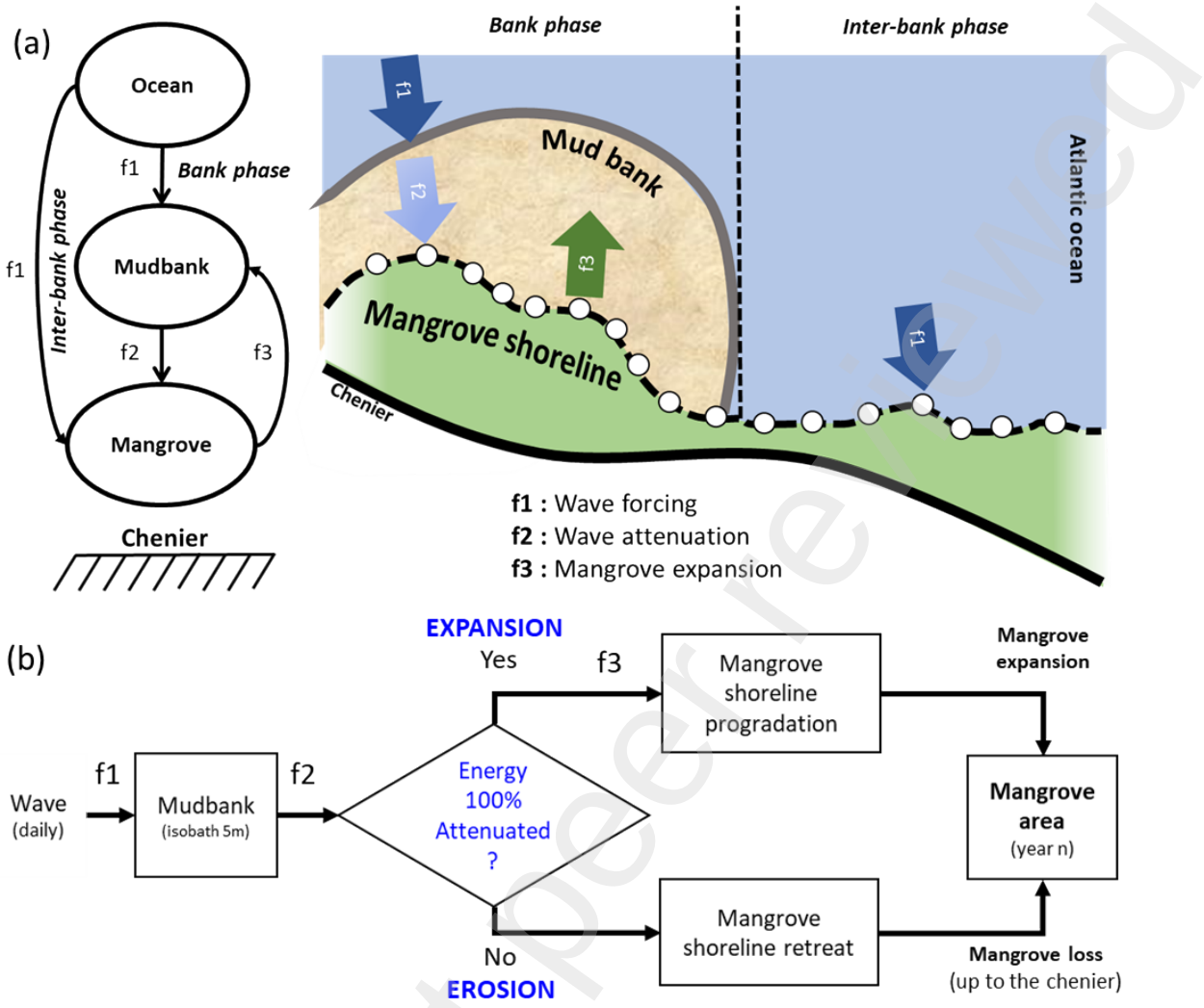


**Fig. 2.** MANG@COAST model design and implementation. (a) Conceptual diagram of the MANG@COAST modeling framework based on entities and relationships. (b) Iterative flowchart diagram of the model for any point on the mangrove shoreline.

The "ocean" entity uses oceanic wave reanalysis data provided by the Copernicus Marine Environment Monitoring Service (CMEMS 2024). The CMEMS wave dataset were collected on a 1/12° grid (approximately 8 km; Fig. 3) between 0°–10 °N and 60°W–40°W and included 3-hourly instantaneous fields of integrated wave parameters. We used the (i) wave height (*VHM0* parameter, in meters), (ii) wave period (*VTPK* parameter, in seconds), and (iii) direction of wave propagation (*MWD* parameter in degrees, meteorological convention). Typically, the wave height and period values provided by the CMEMS data along the coast of French Guiana range from 0.5 to 2 meters and 5 to 20 s respectively; this agrees with literature data and measurements made from a buoy near Cayenne (Fig. A.1; Fig. A.2; Appendix A1). We then estimated the wave energy $E_w$, expressed in $m^3.s^{-2}$, as proposed by Gratiot et al. (2007), for each value of VHM0 and VTPK as follows:

$$E_w = \frac{VHM0^3}{VTPK^2} \quad \text{(Eq. 1).}$$

The wave energy values were then centered and scaled to obtain a forcing signal without units. The direction of wave propagation $D_w$ was obtained by converting the MWD values with angles expressed in degrees to the trigonometric convention, i.e., values of 0° and 90° indicated waves coming from the west and south.

$$D_w = \mathrm{mod}(90\text{-}MWD,360) \quad \text{(Eq. 2)},$$

where $b$=mod($x$,$y$) is the modulo operation which can be expressed as $b = a - y*\mathrm{floor}(x/y)$.

The “mud bank” entity uses annual data from 2011 to 2022 on the extent of mud banks along the entire coast of French Guiana, provided as sets of polygonal vector features (Fig. A.3).

The “mangrove” entity used sets of polygonal vector features that delineate the extent of mangrove cover along the 200 km of the study region for each year between 2011 and 2023 (Fig. A.3). Mangrove shorelines were delineated using visual interpretation of optical and radar satellite images (Table A.1).

The “chenier” entity corresponds to a vector line that was delineated based on visual analysis of remotely sensed imagery capable of distinguishing mangroves from chenier vegetation (Fig. 3).

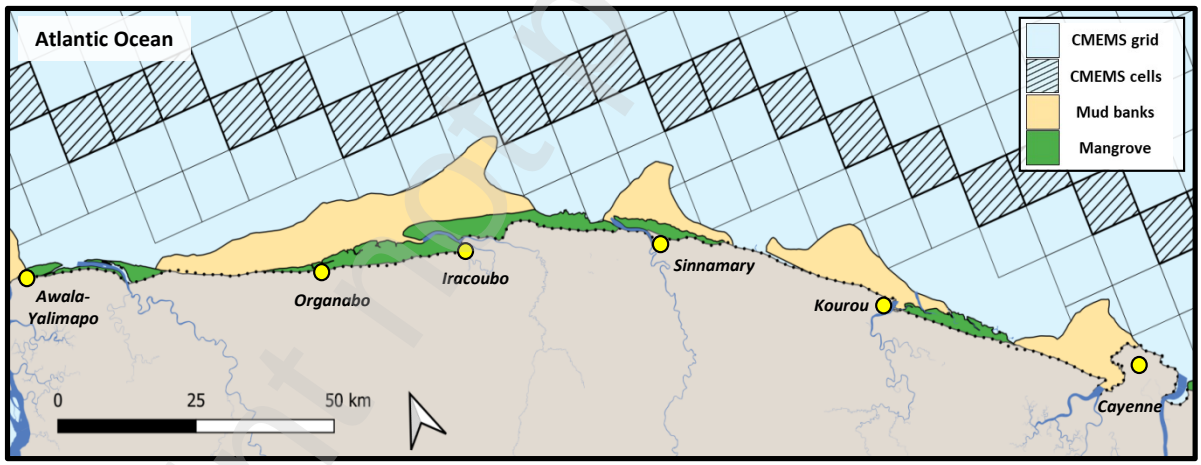


**Fig. 3.** Geographical sketch of entities in 2022. Dashed black line corresponds to the "chenier", the spatial boundary between the mangrove and the land.

### *2.3.3 Relations*

An empirical and simple formulation consistent with our current understanding and observations of wave attenuation by mud banks was used to counterbalance the existing, but almost impossible, parameterization of physical equations. The mangrove retreat, $R$, calculated in meters per day, is

described as a function of the modulus of the wave force $\vec{E}_w$ of energy *E* approaching the coast at an angle $D_w$ *as follows:*

$$R = F_{exposure} * Sf_w * |\vec{E}_w| \quad with \quad F_{exposure} = \left(1 - \frac{d_{att}}{5000}\right)^n \quad \text{(Eq. 3)},$$

where $Sf_w$ is a scale factor, expressed in meters per day, to be estimated by the minimization process described below, and $F_{exposure}$ which represents the wave attenuation effect induced by the muddy bottom of the mud bank (Abascal Zorrilla et al. 2018; Dalrymple and Liu 1978). If the distance $d_{att}$ between the seaward delineation of the mud bank and the seaward mangrove front is greater than 5 km, the wave energy was assumed to be fully attenuated. Otherwise, the wave energy is reduced by $F_{exposure}$, which is modulated by the value of parameter $n$ to be estimated through minimization (Fig. 4).

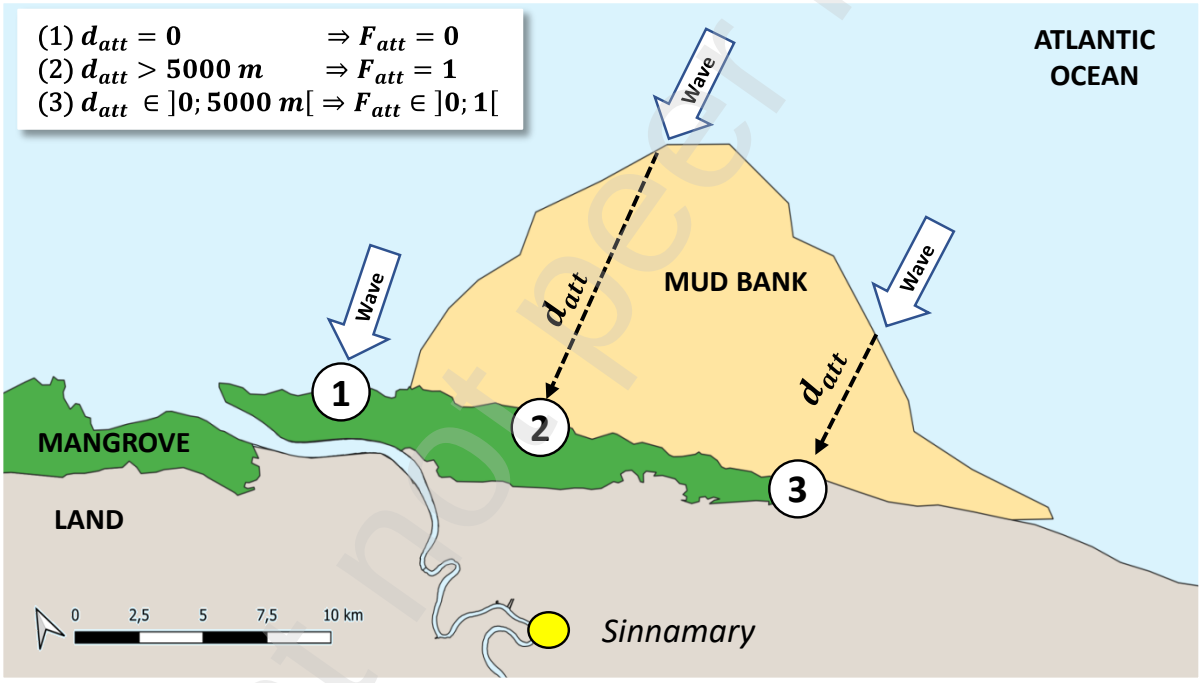


**Fig. 4.** Illustrative real case study depicting how the model works to calculate wave attenuation by a mud bank as a function of the distance $d_{att}$.

The seaward expansion of the mangroves, *S*, is described by a constant equation involving $\beta_{col}$, a parameter the value of which must be obtained by the minimization process, and the local cross-shore direction $\overrightarrow{CC}$ :

$$S = \beta_{col} * \overrightarrow{CC} \quad \text{(Eq. 4)}.$$

At each point protected by the mud bank, the mangrove expansion process must wait for two years, during which 100% of the wave energy must be continuously attenuated. This delay was necessary to allow the mud surface to rise and consolidate (Anthony et al. 2008; Fiot and Gratiot 2006; Gensac et

al. 2015; Proisy et al. 2009). Although the description of the seaward expansion of mangroves on mudflats as a constant function perpendicular to the overall coastal orientation is rudimentary, it corresponds well with our observations of the phenomenon as depicted in satellite images taken each year.

## 2.4 Simulating with MANG@COAST

To simulate mangrove coastlines with MANG@COAST, an interface that can be coded in any programming language such as Python, R or Matlab® is required to (1) set the initial parameter values, (2) handle the minimization process that searches for the best solution, i.e. the parameter values that lead to the minimum error, and (3) exploit the MANG@COAST outputs. We do not describe these programs because we consider them elementary and dependent on user language preferences.

### *2.4.1 Model initiation*

Preliminary values for these three parameters were necessary to initiate the model (Table 1). With regard to mangrove retreat, the acceptable range for $Sf_w$ was established as 0–3 m per day with an initial value of 1.5 m per day (Table 1). This was done to guarantee that wave forcing (f1) affecting the seaward boundary of the mud bank (Fig.2) did not result in simulated mangrove retreat rates exceeding 1095 (3 × 365) m per year in the absence of wave attenuation by a mud bank ($F_{exposure}$ =1 with $d_{att}$=0). The model maintained a certain degree of flexibility in comparison with the observed range of 500 m per year since 1950.

For parameter *n,* the permissible range was set between 0 and 20 with an initial value of 3. It was challenging to set the range of values for *n* because of the limited number of experimental studies on the attenuation effect of waves by mud banks. However, we verified that the MANG@COAST values of *n* were consistent with the nearshore component (Appendix B) of the only available model for wave attenuation in this region (Winterwerp et al. 2007).

**Table 1.** Initial values and valid range for the three parameters of the model. $Sf_w$ and $n$ are employed to simulate the mangrove retreat, while $\beta_{col}$ is used for the mangrove seaward expansion.

| | Initial values | Valid range | Simulated mangrove shoreline change [m/year] |
|---|---|---|---|
| $Sf_w$ | 1.5 | 0 – 3 m/day | [0 – 1095] |
| $n$ | 3 | 0 - 20 | |
| $\beta_{col}$ | 1.5 | 0 – 3 m/day | [0 – 1095] |

For controlling the parameters values of $\beta_{col}$, we set the initial value to 1.5 and an acceptable range of values to [0–3] to allow a maximum seaward mangrove expansion of 1000 m per year, the observed maximum range of expansion being about 400 m per year (Proisy et al. 2021).

### *2.4.2 Minimizing the differences between simulated and observed mangrove areas*

In order to achieve the optimal alignment between the simulated and observed mangrove surface areas, the values of the three parameters $Sf_w$, $\beta_{col}$, and $n$ of the aforementioned two equations are refined through an iterative process based on the surface area encompassed by the union of relative complements of each mangrove area. The cost function used for minimization was defined for a given year as the symmetric difference, *SD*, computed using an XOR operation of the simulated and observed mangrove areas within a given spatial sector (Fig. 5). Different scenarios with varying time steps and spatial extents were used, as described below. The downhill simplex method proposed by Nelder and Mead (1965) was employed to identify the optimal parameter values and facilitate the optimization process.

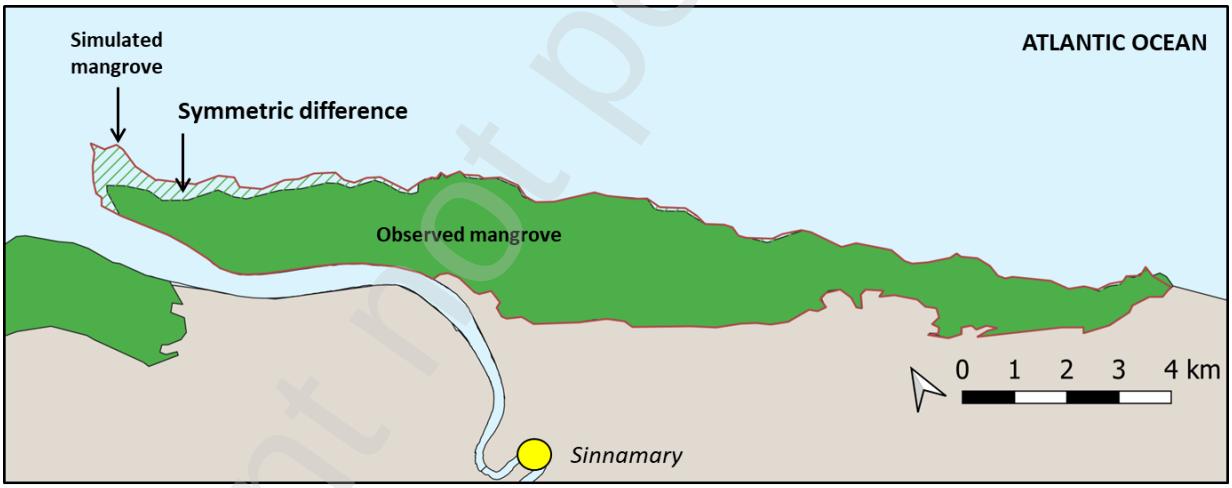


**Fig. 5.** Illustration of the symmetric difference of the simulated and observed mangrove areas for the Sinnamary sector. The calibration process attempts to minimize the magnitude difference.

### *2.4.3 Scenario settings*

Various scenarios were presented to gain insight into how the processes responsible for mangrove retreat during the inter-bank phase or seaward expansion during the bank phase vary in terms of both space and time. The objective of this study was to assess how MANG@COAST simulates the impact of these opposing processes on mangrove shoreline fluctuations in a specific spatial sector within a 10-year period from 2013 to 2023. During this period, annual observations of the mud bank locations and

extents were imposed during the minimization process carried out for all spatial and temporal scenarios.

First, a series of alternative geographical sectors with varying footprints was proposed. The 'regional' sector encompasses the entire 200 km coastline under analysis (Fig. 6a). The "north" and "south" sectors divide the coastline at the point where the coastal orientation changes (Fig. 6b). These two sectors are also divided into sub-sectors, numbered from 1 to 5 (Fig. 6c). These eight spatial scenarios allowed us to consider the north-westward displacement of the bank or interbank phases together or separately (see Table 2). Furthermore, transitional phases were observed, encompassing transitions from a bank to an interbank or an interbank to a bank phase across a range of spatial sectors.

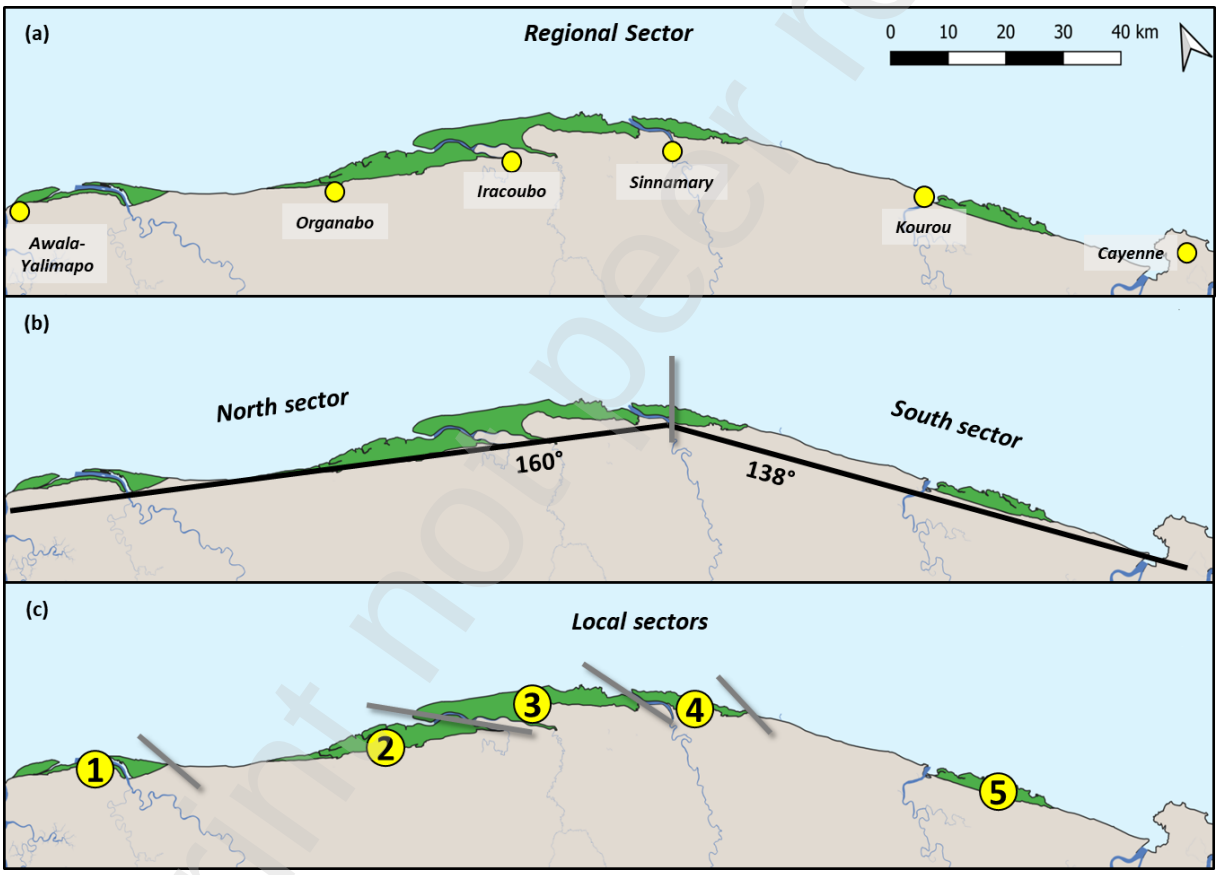


**Fig. 6.** Geographical sectors used in the MANG@COAST scenarios. (a) Regional sector of approximately 200 km. (b) North and south sectors separated by a grey line where the orientation of the shoreline changes (Sinnamary region). Latter is indicated by the bold black line. (c) Local sectors also separated by grey lines are numbered. Mangrove areas are green.

Furthermore, we conducted annual, five-year, and ten-year simulations for each spatial scenario to definitively assess the model's capability to predict fluctuations observed in mangrove shorelines with varying timeframes. The annual scenario was designed to reduce the annual differences between the simulated and observed mangrove surface areas between 2013 and 2023. In

the 5-year and 10-year year scenarios, the values of the three parameters were calculated twice and once from 2013-2023.

**Table 2.** Succession of bank (square), interbank (cross), and transitional (diamond) phases for each sector (see Figure 6) during the 2013-2023 period.

| | Awala | Organabo | Iracoubo | Sinnamary | Cayenne | North | South | Regional |
|---|---|---|---|---|---|---|---|---|
| **2013** | □ | □ | □ | ◊ | □ | □ | ◊ | ◊ |
| **2014** | □ | □ | □ | ◊ | □ | □ | ◊ | ◊ |
| **2015** | ◊ | □ | □ | X | □ | ◊ | ◊ | ◊ |
| **2016** | ◊ | □ | □ | X | □ | ◊ | ◊ | ◊ |
| **2017** | ◊ | □ | □ | ◊ | □ | ◊ | ◊ | ◊ |
| **2018** | ◊ | □ | □ | ◊ | ◊ | ◊ | ◊ | ◊ |
| **2019** | ◊ | □ | □ | ◊ | □ | ◊ | ◊ | ◊ |
| **2020** | X | □ | □ | ◊ | □ | ◊ | ◊ | ◊ |
| **2021** | X | □ | ◊ | □ | ◊ | ◊ | ◊ | ◊ |
| **2022** | X | □ | ◊ | □ | ◊ | ◊ | ◊ | ◊ |
| **2023** | X | □ | ◊ | □ | ◊ | ◊ | ◊ | ◊ |

### *2.4.4 Evaluation of model performance*

We quantitatively evaluated MANG@COAST performance using two indicators and visualized the simulated mangrove shorelines.

The error, *E*, expressed in hectares per kilometer of coastline, was calculated annually as the mean value of the symmetric differences between the simulated and observed mangrove areas $SD_k$ obtained for each kilometer of coastline *k* in a given spatial sector. The calculations are as follows:

$$E = mean\ (SD_k) \text{ (Eq. 5).}$$

To provide a visual idea, a difference of 10 ha per km of coastline between the simulated and observed areas corresponds to an error of ~100 m propagated along one km of the coastline.

The erosion rate indicator, *Ri*, was calculated by comparing the displacements of each kilometer of two successive coastlines, with only the displacements toward the chenier accounted for. The *Ri* values were expressed in meters per year to allow for interpretation and comparability between datasets. This was performed directly on an annual basis for the observed mangrove shorelines, while the daily values of the simulated erosion rates were multiplied by 365, as given in the following equation:

$$R_i = average\ (Sh_{t,k} - Sh_{t-1,k}) \text{ x } 365 \text{ (Eq. 6),}$$

where $Sh_{t,k}\ and\ Sh_{t-1,k}$ are two mangrove shorelines simulated at times *t* and *t-1* on a kilometric portion *k*.

Because the simulated mangrove shorelines can be exported in ESRI Shapefile format, the MANG@COAST outputs can be readily visualized using GIS software.

## 3. Results

Notably, the iteration process converges, indicating that our modeling formulation and implementation are adequate to explain the variability of mangrove shorelines to some extent, which needs to be evaluated. This is consistent with the results of Proisy et al. (2016), who used a more complex formulation based on three relationships and five parameters, without a data set on mudflat areas.

### 3.1. Simulation performance

A machine equipped with an Intel® Core i7-4900MQ processor working at 2.80GHz and 32 Gb of RAM was used to carry out the calculations on Windows 10. The amount of RAM necessary was always less than 5 Gb, including the memory used by our MATLAB® interface and the MANG@COAST Java archive. The computation time to complete an iteration, that is the daily calculation of new mangrove shorelines over one year, did not exceed one minute, regardless of the geographical sector. Convergence is reached after approximately 100 iterations, i.e. about one and a half is required to find the best set of three coefficients for a period of one year.

For the annual scenario, the error values, E, between the simulated and the observed mangrove shorelines varied between 1.6 and 18.4 ha per kilometer of coastline with an average value of 8.1 ha/km ± 3.6 ha/km (Table 2).

**Table 2.** Errors between observed and simulated mangrove shorelines during 2013–2023 considering the annual scenario and the different geographical sectors. Means and standard deviations for the whole period are shown in the last two rows. Bold and italics indicate the minimum and maximum values of *E*.

| *E* [ha/km] | AWALA | ORGANABO | IRACOUBO | SINNAMARY | MACOURIA | NORTH | SOUTH | REGIONAL |
|---|---|---|---|---|---|---|---|---|
| 2013-2014 | 7.2 | 5.7 | *11.4* | *13.3* | 8.2 | 8.1 | *12.2* | *10.1* |
| 2014-2015 | 5.6 | **2.6** | 6.3 | 9.0 | 4.2 | 4.7 | 7.3 | 5.6 |
| 2015-2016 | 7.7 | 4.9 | *18.3* | *18.4* | 4.7 | *11.0* | *11.4* | *11.3* |
| 2016-2017 | 6.1 | **3.1** | *11.1* | *17.0* | **2.7** | 7.3 | 8.8 | 8.0 |
| 2017-2018 | 7.6 | **2.1** | 8.6 | *16.4* | 5.3 | 6.5 | 9.8 | 7.6 |
| 2018-2019 | 6.0 | 9.2 | *14.1* | 9.4 | 6.0 | *10.3* | 8.1 | *10.0* |
| 2019-2020 | 6.3 | **2.8** | 8.5 | 5.1 | 9.5 | 5.8 | 8.1 | 6.6 |
| 2020-2021 | *11.6* | **3.0** | 8.9 | 5.6 | *14.1* | 7.5 | *10.7* | 8.6 |
| 2021-2022 | *12.8* | **3.4** | 8.7 | **1.6** | 6.8 | 7.8 | 4.7 | 6.8 |
| 2022-2023 | *12.2* | **3.2** | 7.0 | **2.4** | 8.0 | 6.9 | 5.8 | 6.5 |
| Mean | 8.3 | **4.0** | *10.3* | 9.8 | 7.0 | 7.6 | 8.7 | 8.1 |
| Standard dev. | 2.8 | 2.1 | 3.6 | 6.2 | 3.2 | 1.9 | 2.4 | 1.9 |

The Iracoubo sector showed the largest average error during 2013–2023, with 10.3 ha/km, while the best performance was obtained for the Organabo sector with an average error of 4 ha/km of coastline. The greatest variability in error was observed for the Sinnamary sector with values ranging from 1.6 to 18.4 ha/km and a standard deviation of 6.2 ha/km. It is noteworthy that the errors obtained for the largest south, north, and regional sectors remained in the same order of magnitude on average, between 7.6 and 8.7 ha/km, as those obtained for the local sectors.

The average error for the five-year scenario is 20.4 ha/km ± 8.3 ha/km, while for the ten-year scenario it is 32.8 ha/km ± 17.8 ha/km of coast (Table 3). Notably, the error levels for the multi-year periods were up to two times greater than those obtained using the annual scenario. The largest error was observed for the Sinnamary sector (80.9 ha/km) in the ten-year scenario. As observed for the annual scenario, there was a minimal increase in the level of error when considering large sectors instead of local sectors during 2013–2023.

**Table 3.** Minimum, mean, and maximum error values considering the 5-year and 10-year scenarios for the different geographical sectors. Bold and italics indicate the minimum and maximum values of *E* for each scenario.

| *E* [ha/km] | 2018-2023 | 2013-2023 |
|---|---|---|
| AWALA | (8.9 ; 19.7 ; 35.9) | (9.7 ; 21.6 ; 41.2) |
| ORGANABO | (9.2 ; 14.6 ; 20.5) | (**5.7** ; 19.9 ; 33.1) |
| IRACOUBO | (15.2 ; 26.6 ; *36.6*) | (11.4 ; 35.6 ; 53.6) |
| SINNAMARY | (9.7 ; 17.7 ; 22.5) | (16.2 ; 56.8 ; *80.9*) |
| MACOURIA | (**7.3** ; 21.9 ; 32.2) | (8.2 ; 22.8 ; 37.3) |
| NORTH | (11.4 ; 21.3 ; 32.2) | (8.6 ; 30.8 ; 45.6) |
| SOUTH | (8.1 ; 20.4 ; 28.5) | (13.8 ; 40.5 ; 59.4) |
| REGIONAL | (10.4 ; 21.2 ; 31.0) | (10.3 ; 34.5 ; 49.9) |

The observed and simulated average and maximum annual erosion rates were compared for the five local sectors from 2013 to 2023 period (Table 4). Based on the phase succession given in Table 2, the bank phases (when mangroves could expand) were distinguished from both the interbank and transitional phases (when mangroves could be eroded).

During the bank phases, the results demonstrated that the erosion rates were accurately simulated across all sectors, with the mean simulated values closely aligned with the observed values, and the maximum simulated erosion rates slightly exceeding the observed values.

During the interbank phases, all simulated erosion rates were higher than those obtained during the bank phases. The mean simulated *Ri* values were of the same magnitude as the observed values. However, the maximum simulated erosion rates for the Iracoubo (689 m/y) and Macouria (524 m/y) sectors were overestimated compared with the observed erosion rates of 80 m/y and 345 m/y, respectively.

**Table 4.** Mean and maximum values of observed and simulated erosion rates for each sector and distinguishing bank from interbank or transitional phases. Bold values indicate close values of observed and simulated erosion rates. Italics indicate significant differences between observed and simulated erosion rates.

| Erosion rates $R_i$ [m. year$^{-1}$] | | AWALA | ORGANABO | IRACOUBO | SINNAMARY | MACOURIA |
|---|---|---|---|---|---|---|
| Bank phase | Observed | ***(*23; *63)*** | **(1; 5)** | **(14; 55)** | **(19; 44)** | **(29; 84)** |
| | Simulated | **(5; *143)*** | **(3; 9)** | **(13; 95)** | **(3; 61)** | **(19; 110)** |
| Interbank-transitional phase | Observed | **(83; *174*)** | (None; None) | *(***25***; 80)* | **(176; *345*)** | **(26; *67)*** |
| | Simulated | **(81; *323*)** | (None; None) | *(***75***; 689)* | **(153; *524*)** | **(41; *343)*** |

## 3.2. Wave attenuation by mud banks

MANG@COAST was designed to simulate the seaward progradation and retreat of mangrove shorelines. The latter process is described by Equation 3, which includes the term $F_{exposure}$, used to quantify the exposure of the mangrove shoreline to waves as a function of the distance $d_{att}$ between the seaward edge of the mud bank and the mangrove shoreline (Fig. 4). The values for the exponent *n* recorded for $d_{att}$<5 km were thus obtained from the minimization process. They can be considered informative of the variability in wave attenuation potential observed in different geographical sectors. Thus, we constructed a quantitative chart of wave attenuation by the mud bank, depending on the extent of the mud bank in front of the mangrove shoreline (Fig. 7). The shape of the attenuation profile $F_{att}$ is calculated as

$$F_{att} = 1 - F_{exp} \text{ (Eq. 6).}$$

As the values found for parameter n were all positive and ranged from 4.42 to 19.07, the model outputs suggest that wave attenuation mainly occurs once the seaward edge of the mud bank was crossed. Over 90% of the wave energy can be attenuated if 600 m < $d_{att} < 2000$ m, regardless of the geographical sector, that is its coastal orientation and the shape of the mud bank. If the extent of the mud bank was greater than 3 km, most of the wave energy was attenuated. Closer to the mangrove seafront, for example, with $d_{att}$ < 500 m, wave energy attenuation can vary from 40% to 90%. This significant variability is discussed below in relation to the morphology and topography of the mud banks.

Our modeling results are consistent with the few *in situ* measurements reported in the literature. At 2000 < $d_{att} < 3000$ m, Abascal Zorrilla et al. (2018) measured an attenuation of 83% of the wave height in French Guiana (Fig. 7). However, our model results in the nearshore domain cannot be compared with those of the model proposed by Winterwerp et al. (2007) to quantify the

attenuation of the ocean by muddy waters off the coast of Guyana, that is, for $d_{att}$ > 5000 m (Appendix B).

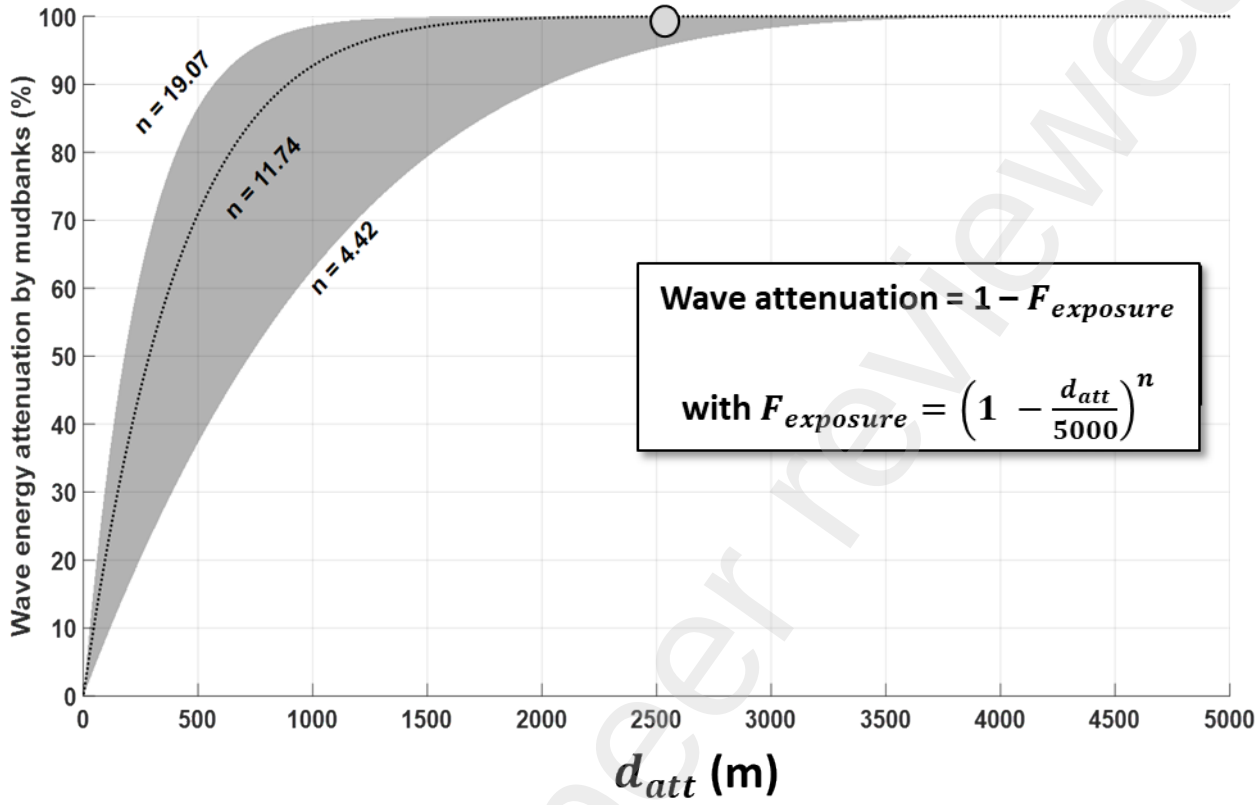


**Figure. 7.** Simulated wave attenuation profiles by mud banks as a function of the distance $d_{att}$ between the seaward edge of the mud bank ($d_{att}$ =0) and the mangrove shoreline ($d_{att}$ =5000). $F_{att}$ values are in percent. Grey circle positioned at 99% of the wave energy attenuation corresponds to the 83% wave height attenuation at datt = 2500 m calculated with a mean wave period of 8 s, as observed in Abascal Zorrilla et al. (2018).

### 3.3. Seasonal variability in mangrove shoreline erosion

The use of the erosion rate Ri, calculated daily by MANG@COAST, provides a unique opportunity to consider the seasonal variability in the magnitude of erosion for each geographical sector. First, as shown in Fig. 8, for two sectors experiencing bank and interbank phases, erosion is significantly reduced by the presence of the mud bank, whereas during the interbank phase, erosion rates, that is mangrove retreat, can reach 400 m per year for the Sinnamary sector. Second, the daily estimates of erosion rates were consistent with the annual range of erosion rates (horizontal lines in the graph). Third, our modeling results highlight that the erosion signal is seasonal, similar to the wave regime approaching the coast of French Guiana, with the most energetic waves occurring between December and May. Overall, the presence of a mud bank is synonymous with mangroves, and more generally, with shoreline protection throughout the year.

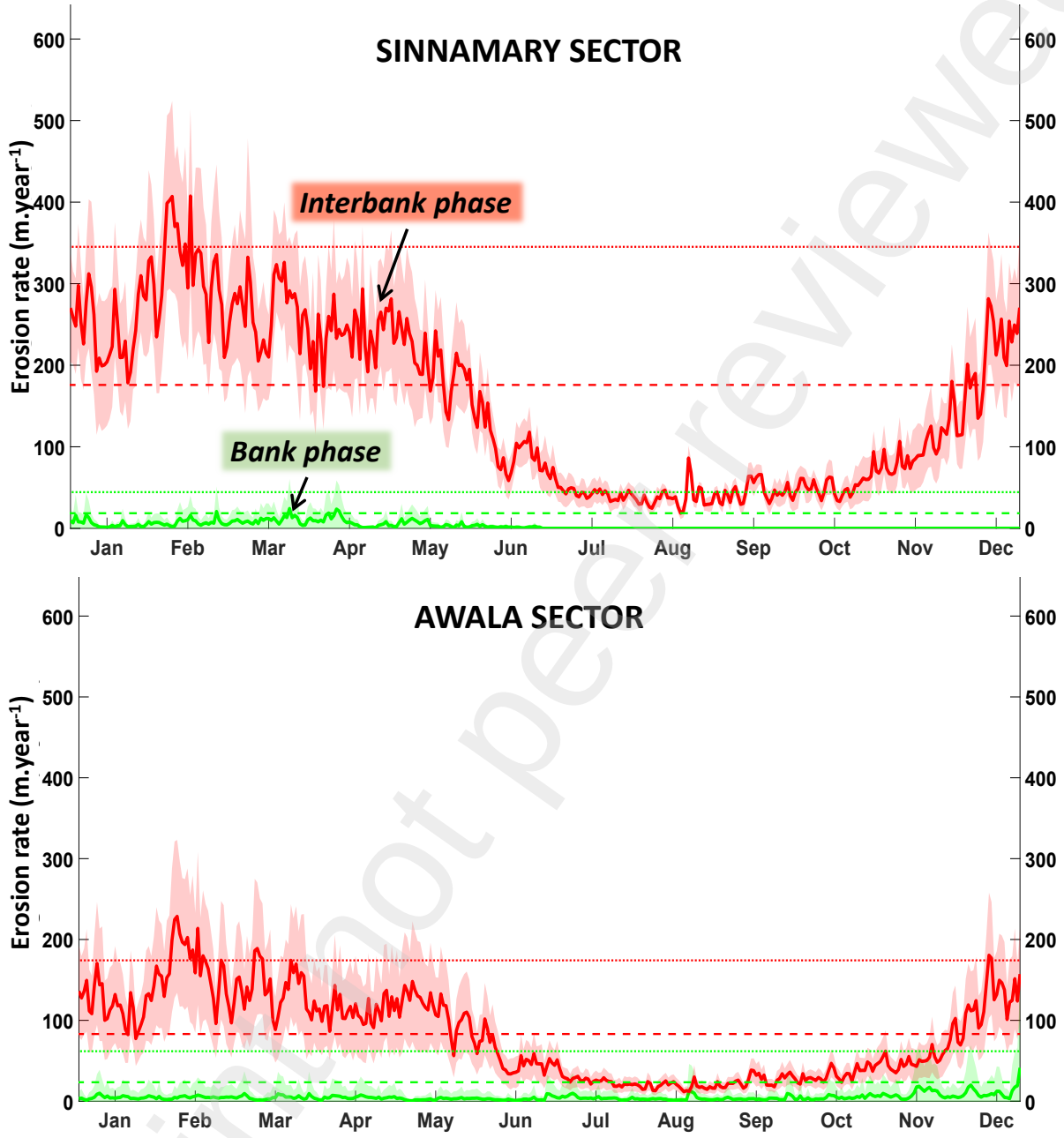


**Figure. 8.** Seasonal erosion (i.e. mangrove retreat) rates simulated for bank and interbank phases for the SINNAMARY and AWALA sectors. Horizontal dotted and dashed lines correspond to the maximum and mean values observed in remote sensing images for both bank and interbank phases.

### 3.4. New quantitative insight for the French Guiana coast

The modeling exercise based on the eight geographical sectors and annual scenarios resulted in 80 values for each of the three parameters for 2013–2023. Here, we analyzed the entire range of values for the three parameters to provide a physical interpretation of the coastal processes that affect the coast of French Guiana (Table 5).

With daily values of the parameter $Sf_w$ varying between 0.6 and 3.0 m, the wave energy attaining the seaward edge of the mud bank can result in erosion rates ranging from 219 to 1095 m/year. As explained above, the analysis of $n$ values indicates that 90% of the wave energy can be attenuated if the extent of the mud bank in front of the mangrove is at least 500 m. However, variability in N values is observed across geographical sectors and years. The values for the parameter $\beta_{col}$, which expresses the rate of seaward expansion of mangroves on the intertidal part of the mud bank, range from 0 to 0.48 meters per day, corresponding to annual expansion rates averaging between 87 and 175 meters, values in agreement with our observations (Gensac et al. 2015; Proisy et al. 2009).

**Table 5.** MANG@COAST parameter values describing the spatial and temporal dynamics of mangroves, over 200 km of coastline between 2013–2023 and their interpretation in terms of coastal processes.

| **2013-2023** | $\mathrm{Sf_w}$ | n | $\boldsymbol{\beta}_{\mathrm{col}}$ |
|---|---|---|---|
| **MANG@COAST parameters** | $1.80 \pm 1.2\ (m./day)$ | $11.7 \pm 7.3$ | $0.3 \pm 0.28\ (m/day)$ |
| **Physical interpretation** | Erosion due to offshore wave forcing 219 and 1105 m/year | Wave attenuation >90% if 600 <$d_{att}$ < 2000 m | Mangrove seaward progradation up to 175 m/year |

## 4. Discussion

### 4.1 How specific is the FG coast in terms of the mangrove-wave attenuation relationship?

In MANG@COAST, the annual fluctuations in mangrove extent observed by remote sensing were modeled as the two opposing processes of mangrove retreat and seaward expansion. These processes are regulated by the presence and spatial characteristics of alongshore migrating mud banks (Anthony et al. 2022). These mud banks mitigate the impact of oceanic waves on the coast. Behind this fairly simple conceptualization is the modeling formalism, its implementation, and the model's ability to correctly simulate what is expected of it. Although accurate modeling of mangrove expansion remains complex and cannot be presented as an average, our preliminary quantitative results suggest that the expansion capacity of mangroves on newly formed mudflats is less than the potential erosive force induced by offshore waves. Mangroves are increasingly subject to erosion as the interbank front approaches the mud bank trailing edge. The extent of mangrove retreat suggests that mud banks assured the primary mechanism of wave attenuation on this relatively high-energy coast.

The mangrove shoreline along the coast of French Guiana would not fluctuate without mud banks of sufficient size to attenuate wave energy. Notably, Brunier et al. (2019) observed that small mud-banks in the Awala sector temporarily impeded shoreline erosion, yet did not facilitate the expansion

of mangrove habitats. In this case, coastal mangroves would disappear. This also implies that the presence and abundance of mangroves on this coast are closely linked to the existence and characteristics of mud banks. We do not suggest that mangroves do not dissipate wave energy. We are simply highlighting the fact that the year-long energetic wave context on the FG coast largely exceeds the intrinsic capacity of mangroves on this coast to dissipate wave energy.

### 4.2 Strengths and limitations of MANG@COAST

We found the interaction graph modeling formalism approach to be intuitive and, in any case, well suited to our need to model processes that are fairly well understood but poorly quantified. The Ocelet approach is particularly attractive because it allows spatial and temporal observations of mangrove shorelines to be manipulated as they occur in a GIS database while focusing on the realistic formulation of any interactions deemed essential according to experimental and qualitative knowledge. The manipulation of entities and interactions not only opens up the possibility of imagining new multiscale modeling approaches for complex environments but also ensures that the model can be updated with any additional knowledge. When upgrading, new formulations of the interactions between existing or new entities can be intuitively proposed without having to redesign the entire model code.

The Ocelet programming language is relatively straightforward (Degenne and Lo Seen 2016). The model code was compiled based on a set of Java classes and libraries, thereby enabling both the inputs and outputs of the model to be processed via interfaces that can be coded in any preferred programming language. Oceanic wave data are accessible for any mangrove coastline from the Copernicus Marine Data store (https://data.marine.copernicus.eu/products). Nevertheless, even if the observational data to be linked to the model can be meticulously prepared directly in GIS, the process of obtaining them from remote-sensing observations requires a significant investment in time and effort. This latter factor must be subjected to rigorous evaluation before embarking on the modeling process. The calculation of annual simulated mangrove areas over 200 km of the coastline from daily records of wave data is a relatively time-consuming process. On a standard machine, it takes ~1.5 h, with no request for RAM to exceed the typical configuration of 16 GB. The mud bank and mangrove data were vectorized, and only the wave data at the nearshore interface were stored. It is recommended that the simulations be batch-processed and that the codes be optimized to enhance efficiency.

The simulation of fluctuations in mangrove extent yielded average errors ranging from 4.5 ha/km for the annual scenario to 56.8 ha per km of coastline for the 10-year scenario for 2013–2023. Errors from the local, northern, and southern sectors to the regional sectors were found to increase slightly.

When temporal scenarios of multiple years were considered, the errors increased significantly. It is recommended that data on the mud bank extent and location be employed annually to adjust the model parameter values. Furthermore, the topography and elevation of the mud bank should be considered when modeling both wave attenuation and mangrove expansion. These are two driving parameters for mudbank consolidation (Anthony et al. 2008) and tidal processes, the latter being responsible for the dispersal of mangrove seeds.

Specifically, the ability of mangroves to expand on a new mud bank remains complex to model (Beselly et al. 2023) and requires fine-scale mapping techniques (Anthony et al. 2008; Proisy et al. 2009). While lidar systems embarked on unmanned aerial systems (UAS) are not yet capable of flying across large areas, repeated UAS-based lidar surveys provide valuable maps of sediment surface elevation and mangrove growth at a very fine scale, with horizontal and vertical accuracy of a few centimeters (Brunier et al. 2016). This is a crucial step for more accurate modeling of mangrove expansion.

There were discrepancies between the simulated and observed mangrove areas around the river mouths, as evidenced by data from the Sinnamary sector. River mouths along the Guiana coast exhibit a physiognomy shaped by the interplay of multiple factors, including the circulation of mud banks from southeast to northwest, the flow of water from the river basin, and the rock type of the fluvial catchment area (Gardel et al. 2022). As MANG@COAST does not consider these additional factors in the vicinity of river mouths, the simulated mangrove landscape around the estuary cannot be accurately aligned with what we observed over hundreds of hectares on an annual basis.

MANG@COAST can be used to gain deeper insight into these processes, which have only been studied to a limited extent and remain to be quantified. A new 'river' entity could be created with a parameterized influence of the river seasonal runoff. During the erosion phases, the potential to attenuate waves northwest of the river mouth could be linked to this new entity in a manner proportional to the discharge of water. However, it may be advisable to base further modeling studies of mangrove landscapes around river mouths on more frequent monitoring to enable simulations at monthly intervals. Notably, a monthly coastal monitoring program based on freely downloadable C-band radar SENTINEL-1 images represents a viable option towards which we already proceed.

Overall, the range of simulated mangrove retreat rates was found to be well within the range of the observed values. This led to the development of a unique and realistic chart for assessing wave energy reduction with respect to mangrove coverage along the mangrove coastline. This chart offers valuable assistance to the French Guiana Coastal Observatory (ODyC), which aims to predict coastal vulnerability to wave erosion.

### 4.3 Potential perspectives

### *4.3.1 Coupling with mangrove forest models*

Further development will link MANG@COAST to existing models of forest dynamics (Berger et al. 2008). This will entail forcing the latter models by coastal processes of sedimentation (start) and erosion (stop) and spatializing their calculations. The MANG@COAST mangrove entity can be rasterized and divided into a grid of cells representative of different forest stands. The calculations of tree growth, biomass, and carbon storage can then be applied to each cell over the period in which coastal processes exert control. Hybrid and fine-scale modeling approaches are required to meet the local challenge of predicting changes along the mangrove coast (Beselly et al. 2023). To achieve this, a strong collaboration among ecology, remote sensing, and modeling scientists is necessary.

### *4.3.2 From French Guiana to the rest of the Amazon-influenced coast*

MANG@COAST was developed in a region spanning approximately 200 km from Cayenne, 120 km north of the boundary with Brazil, to the mouth of the Maroni River at the boundary with Suriname. This region did not cover the entire 320 km long coast of French Guiana. Indeed, it was premature to model the southern part of the French Guiana coast because mud banks that form at the boundary with Brazil cannot be well individualized; that is, their interactions with the large Approuague and Oyapock River waters are insufficiently described, partly due to a lack of field data and remote sensing observations on muddy waters (Anthony et al. 2022). The influence of both river waters and the rock type of the fluvial catchment on the shape of the mangrove coast must be integrated into any further modeling objective.

MANG@COAST can be applied with the same modeling entities and data types to the coasts of Suriname (de Vries et al. 2022) and Guyana (Anthony and Gratiot 2012; Best et al. 2022), which collectively account for approximately 800 km of the 1500 km-long mud-dominated Amazon-influenced coastlines.

MANG@COAST can be applied, at least in part, to the open coast of Amapá, Brazil, which extends more than 450 km south of French Guiana (Fig. 1), from the mouth of the Oyapock to the Amazon rivers (Allison et al. 1995). The processes of seaward mangrove expansion and mangrove retreat that occur in the muddy capes of Orange and Cassiporé, near the border with French Guiana, lends themselves well to modeling. To the south, sandy sediments with intercalated mud plains dominate, without significant seaward mangrove expansion (Santos et al. 2016). The most extensive mangrove area on the Amazon coast is in the Cabo Norte region at the mouth of the Amazon River. Extreme, rapid, and high-magnitude coastal processes under macrotidal regimes (Beardsley et al. 1995), including tidal bores, affect the entire mangrove coastline (Allison et al. 1995). Observational data on

tides and river discharge are required to integrate new entities and their relationships into a satisfactory modeling approach involving additional new entities.

#### *4.3.3 For global and long-term predictions*

A global version of MANG@COAST can be developed to link maps of changes in mangrove extent provided by the Global Mangrove Watch initiative (Bunting et al. 2022). This version can be prepared to integrate generic equations forced by one or two entities corresponding to the most prevalent drivers of changes in mangrove extent for a given coast. The first objective of the global version of the present MANG@COAST model would be to test the causality of physical processes induced by climate change (e.g., wave and wind regimes) on mangrove retreat and destruction rates.

However, a semi-empirical modeling approach is not a panacea for the nonstationary nature of coastal processes. Even if muddy coasts can be monitored in three dimensions, the multiscale intertwining of complex processes will remain a challenge for predicting coastal changes over the next few years.

## 5. Conclusion

We implemented and tested the MANG@COAST modeling approach to propose an initial tool for simulating the dynamics of the unique coastal mangrove landscape of French Guiana. Similar to other models, MANG@COAST has both strengths and weaknesses. However, it offers insights into potential applications for a better understanding of mangrove-mud bank-wave attenuation relationships and their implications for enhanced coastal management in French Guiana and its regions. This study demonstrates how monitoring healthy and highly dynamic mangrove landscapes in a protected area can help anticipate coastal changes in the short term and consequently address the potential economic and physical impacts on coastal livelihoods.

We predicted coastal vulnerability to erosion by improving our modeling of mangrove establishment and sediment attachment to the coast. Based on this, we actually provided a concrete framework to support a nature-based solutions approach (Seddon et al. 2021) for mangrove coasts, where innovative and interdisciplinary modeling initiatives are necessary to research components to meet the challenge of adaptation to climate change and biodiversity loss. Above all, international action is required to maintain a sufficient sediment supply to the coast, providing mangroves with the shelter they need to develop on any coast in the world.

**Acknowledgments**

Paul-Emile Augusseau benefited from a doctoral fellowship from the Public Industrial and Commercial Establishment (ADEME) and the General Directorate for Territories and the Sea of French Guiana (DGTM). Adrien Staquet received a doctoral fellowship from the Priority Research Programme "Oceans and Climate" led by the French National Centre for Scientific Research (CNRS) and the French Research Institute for the Exploitation of the Sea (IFREMER). Romain Walcker acknowledges the financial support he received from the French National Research Agency through the Investissement d'Avenir program (Labex CEBA, ref.ANR-10-LABX-25-01). This work was a part of the Living Labs project funded by the France 2030 program on Nature-based Solutions (ANR-22-EXSO-0002). The study was conducted using marine data provided by the E.U. Copernicus Marine Service Information https://data.marine.copernicus.eu/products, including the "Global Ocean Waves Analysis and Forecast" (https://doi.org/10.48670/moi-00017 and https://doi.org/10.48670/moi-00022) and Suspended Particulate Matter (https://doi.org/10.48670/moi-00281). We thank Noelia Abascal Zorilla and the "Observatoire de la Dynamique Cotière" (ODyC; https://observatoire-littoral-guyane.fr/) for providing essential data for mud bank delimitation.

**References**

Abascal Zorrilla N., Vantrepotte V., Gensac E., Huybrechts N. and Gardel A., 2018. The Advantages of Landsat 8-OLI-Derived Suspended Particulate Matter Maps for Monitoring the Subtidal Extension of Amazonian Coastal Mud Banks (French Guiana). Remote Sensing. 10, 1733. https://doi.org/10.3390/rs10111733

Allison M.A., Nittrouer C.A. and Faria L.E.C., 1995. Rates and mechanisms of shoreface progradation and retreat downdrift of the Amazon river mouth. Marine Geology. 125, pp. 373-392. https://doi.org/10.1016/0025-3227(95)00020-Y

Anthony E.J., Dolique F., Gardel A., Gratiot N., Proisy C. and Polidori L., 2008. Nearshore intertidal topography and topographic-forcing mechanisms of an Amazon-derived mud bank in French Guiana. Continental Shelf Research. 28, 813-822. https://doi.org/10.1016/j.csr.2008.01.003

Anthony E.J., Gardel A., Gratiot N., Proisy C., Allison M.A., Dolique F. and Fromard F., 2010. The Amazon-influenced muddy coast of South America: A review of mud-bank–shoreline interactions. Earth-Science Reviews. 103, pp. 99-121. https://doi.org/10.1016/j.earscirev.2010.09.008

Anthony E.J., Gardel A., Zainescu F. and Brunier G., 2022. 8.15 - Fine Sediment Systems, in: J. F. Shroder (Eds.), Treatise on Geomorphology (Second Edition), 465-493, https://doi.org/10.1016/B978-0-12-818234-5.00130-9

Anthony E.J. and Gratiot N., 2012. Coastal engineering and large-scale mangrove destruction in Guyana, South America: Averting an environmental catastrophe in the making. Ecological Engineering. 47, pp. 268-273. https://doi.org/10.1016/j.ecoleng.2012.07.005

Beardsley R.C., Candela J., Limeburner R., Geyer W.R., Lentz S.J., Castro B.M., Cacchione D. and Carneiro N., 1995. The M2 tide on the Amazon Shelf. Journal of Geophysical Research: Oceans. 100, pp. 2283-2319. https://doi.org/10.1029/94JC01688

Berger U., Rivera-Monroy V.H., Doyle T.W., Dahdouh-Guebas F., Duke N.C., Fontalvo-Herazo M.L., Hildenbrandt H., Koedam N., Mehlig U., Piou C. and Twilley R.R., 2008. Advances and limitations

of individual-based models to analyze and predict dynamics of mangrove forests: A review. Aquatic Botany. 89, pp. 260-274. https://doi.org/10.1016/j.aquabot.2007.12.015

Beselly S.M., Grueters U., van Der Wegen M., Reyns J., Dijkstra J. and Roelvink D., 2023. Modelling mangrove-mudflat dynamics with a coupled individual-based-hydro-morphodynamic model. Environmental Modelling & Software. 169, 105814. https://doi.org/10.1016/j.envsoft.2023.105814

Besset M., Gratiot N., Anthony E.J., Bouchette F., Goichot M. and Marchesiello P., 2019. Mangroves and shoreline erosion in the Mekong River delta, Viet Nam. Estuarine, Coastal and Shelf Science. 226, 106263. https://doi.org/10.1016/j.ecss.2019.106263

Best Ü.S.N., van der Wegen M., Dijkstra J., Reyns J., van Prooijen B.C. and Roelvink D., 2022. Wave attenuation potential, sediment properties and mangrove growth dynamics data over Guyana's intertidal mudflats: assessing the potential of mangrove restoration works. Earth System Science Data 14, pp. 2445–2462. https://doi.org/10.5194/essd-14-2445-2022

Blasco F., Saenger P. and Janodet E., 1996. Mangroves as indicators of coastal change. CATENA. 27, 167-178. https://doi.org/10.1016/0341-8162(96)00013-6

Brunier G., Anthony E.J., Gratiot N. and Gardel A., 2019. Exceptional rates and mechanisms of muddy shoreline retreat following mangrove removal. Earth Surface Processes and Landforms. 44, 1559-1571. https://doi.org/10.1002/esp.4593

Brunier G., Fleury J., Anthony E.J., Pothin V., Vella C., Dussouillez P., Gardel A. and Michaud E., 2016. Structure-from-Motion photogrammetry for high-resolution coastal and fluvial geomorphic surveys. Géomorphologie : relief, processus, environnement. 22, 147-161. https://doi.org/10.4000/geomorphologie.11358

Bunting P., Rosenqvist A., Hilarides L., Lucas R.M. and Thomas N., 2022. Global Mangrove Watch: Updated 2010 Mangrove Forest Extent (v2.5). Remote Sensing. 14, 1034. https://doi.org/10.3390/rs14041034

Castelle B., Ritz A., Marieu V., Nicolae Lerma A. and Vandenhove M., 2022. Primary drivers of multidecadal spatial and temporal patterns of shoreline change derived from optical satellite imagery. Geomorphology. 413, 108360. https://doi.org/10.1016/j.geomorph.2022.108360

CMEMS, 2024. Copernicus Marine Environment Monitoring Service. https://data.marine.copernicus.eu/products.

Dalrymple R.A. and Liu P.L.F., 1978. Waves over Soft Muds: A Two-Layer Fluid Model. Journal of Physical Oceanography. 8, pp. 1121-1131. https://doi.org/10.1175/1520-0485(1978)008<1121:WOSMAT>2.0.CO;2

de Vries J., van Maanen B., Ruessink G., Verweij P.A. and de Jong S.M., 2022. Multi-decadal coastline dynamics in Suriname controlled by migrating subtidal mudbanks. Earth Surface Processes and Landforms. 47, pp. 2500-2517. https://doi.org/10.1002/esp.5390

Degenne P. and Lo Seen D., 2016. Ocelet: Simulating processes of landscape changes using interaction graphs. SoftwareX. 5, pp. 89-95. https://doi.org/10.1016/j.softx.2016.05.002

Degenne P., Lo Seen D., Parigot D., Forax R., Tran A., Ait Lahcen A., Curé O. and Jeansoulin R., 2009. Design of a Domain Specific Language for modelling processes in landscapes. Ecological Modelling. 220, pp. 3527-3535. https://doi.org/10.1016/j.ecolmodel.2009.06.018

Ellison J.C., 2019. Chapter 20 - Biogeomorphology of Mangroves, in: G. M. E. Perillo, E. Wolanski, D. R. Cahoon and C. S. Hopkinson (Eds.), Coastal Wetlands (Second Edition), pp. 687-715, https://doi.org/10.1016/B978-0-444-63893-9.00020-4

Fiot J. and Gratiot N., 2006. Structural effects of tidal exposures on mudflats along the French Guiana coast. Marine Geology. 228, pp. 25-37. https://doi.org/10.1016/j.margeo.2005.12.009

Foster-Martinez M.R., Alizad K. and Hagen S.C., 2020. Estimating wave attenuation at the coastal land margin with a GIS toolbox. Environmental Modelling & Software. 132, 104788. https://doi.org/10.1016/j.envsoft.2020.104788

Froidefond J.M., Pujos M. and Andre X., 1988. Migration of mud banks and changing coastline in French Guiana. Marine Geology. 84, pp. 19-30. https://doi.org/10.1016/0025-3227(88)90122-3

Gao S., 2019. Chapter 10 - Geomorphology and Sedimentology of Tidal Flats, in: G. M. E. Perillo, E. Wolanski, D. R. Cahoon and C. S. Hopkinson (Eds.), Coastal Wetlands (Second Edition), pp. 359-381, https://doi.org/10.1016/B978-0-444-63893-9.00010-1

Gardel A., Anthony E.J., Santos V.F., Huybrechts N., Lesourd S., Sottolichio A. and Maury T., 2022. A remote sensing-based classification approach for river mouths of the Amazon-influenced Guianas coast. Regional Environmental Change. 22, 65. http://doi.org/10.1007/s10113-022-01913-3

Gedan K.B., Kirwan M.L., Wolanski E., Barbier E.B. and Silliman B.R., 2011. The present and future role of coastal wetland vegetation in protecting shorelines: answering recent challenges to the paradigm. Climatic Change. 106, pp. 7-29. https://doi.org/10.1007/s10584-010-0003-7

Gensac E., Gardel A., Lesourd S. and Brutier L., 2015. Morphodynamic evolution of an intertidal mudflat under the influence of Amazon sediment supply – Kourou mud bank, French Guiana, South America. Estuarine, Coastal and Shelf Science. 158, pp. 53-62. https://doi.org/10.1016/j.ecss.2015.03.017

Gensac E., Martinez J.-M., Vantrepotte V. and Anthony E.J., 2016. Seasonal and inter-annual dynamics of suspended sediment at the mouth of the Amazon river: The role of continental and oceanic forcing, and implications for coastal geomorphology and mud bank formation. Continental Shelf Research. 118, pp. 49-62. https://doi.org/10.1016/j.csr.2016.02.009

Ghosh S., Proisy C., Muthusankar G., Hassenrück C., Helfer V., Mathevet R., Andrieu J., Balachandran N. and Narendran R., 2022. Multiscale Diagnosis of Mangrove Status in Data-Poor Context Using Very High Spatial Resolution Satellite Images: A Case Study in Pichavaram Mangrove Forest, Tamil Nadu, India. Remote Sensing. 14, 2317. https://doi.org/10.3390/rs14102317

Gratiot N. and Anthony E.J., 2016. Role of flocculation and settling processes in development of the mangrove-colonized, Amazon-influenced mud-bank coast of South America. Marine Geology. 373, pp. 1-10. https://doi.org/10.1016/j.margeo.2015.12.013

Gratiot N., Gardel A. and Anthony E.J., 2007. Trade-wind waves and mud dynamics on the French Guiana coast, South America: Input from ERA-40 wave data and field investigations. Marine Geology. 236, pp. 15-26. https://doi.org/10.1016/j.margeo.2006.09.013

Hulskamp R., Luijendijk A., van Maren B., Moreno-Rodenas A., Calkoen F., Kras E., Lhermitte S. and Aarninkhof S., 2023. Global distribution and dynamics of muddy coasts. Nature Communications. 14, 8259. https://doi.org/10.1038/s41467-023-43819-6

Jahel C., Augusseau X. and Lo Seen D., 2018. Modelling cropping plan strategies: What decision margin for farmers in Burkina Faso? Agricultural Systems. 167, pp. 17-33. https://doi.org/10.1016/j.agsy.2018.08.004

Jain M. and Mehta A.J., 2009. Role of basic rheological models in determination of wave attenuation over muddy seabeds. Continental Shelf Research. 29, pp. 642-651. https://doi.org/10.1016/j.csr.2008.09.008

Mazda Y., Wolanski E. and Ridd P., 2007. The Role of Physical Processes in Mangrove Environments: manual for the preservation and utilization of mangrove ecosystems. TERRAPUB.

McGranahan G., Balk D. and Anderson B., 2007. The rising tide: assessing the risks of climate change and human settlements in low elevation coastal zones. Environment and Urbanization. 19, pp. 17-37. https://doi.org/10.1177/0956247807076960

Mehta A.J., 2002. Chapter Three Mudshore dynamics and controls, in: T. Healy, Y. Wang and J.-A. Healy (Eds.), Proceedings in Marine Science, pp. 19-60, https://doi.org/10.1016/S1568-2692(02)80077-8

Nelder J.A. and Mead R., 1965. A Simplex Method for Function Minimization. The Computer Journal. 7, pp. 308-313. https://doi.org/10.1093/comjnl/7.4.308

Proisy C., Degenne P., Anthony E.J., Berger U., Blanchard E., Fromard F., Gardel A., Olagoke A., Santos V.F., Walcker R. and Lo Seen D., 2016. A Multiscale Simulation Approach for Linking Mangrove Dynamics to Coastal Processes using Remote Sensing Observations. Journal of Coastal Research. 75, pp. 810-814. https://doi.org/10.2112/SI75-163.1

Proisy C., Gardel A., Blanchard F. and Staquet A., 2022. Mangroves and coastal dynamics on French Guiana's coast. Fondation de l'Université de Guyane & ADEME. https://www.calameo.com/read/006821969cd067f7a1074

Proisy C., Gratiot N., Anthony E.J., Gardel A., Fromard F. and Heuret P., 2009. Mud bank colonization by opportunistic mangroves: A case study from French Guiana using lidar data. Continental Shelf Research. 29, pp. 632-641. https://doi.org/10.1016/j.csr.2008.09.017

Proisy C., Walcker R., Blanchard E., Gardel A. and Anthony E.J., 2021. Chapter 2 - Mangroves: a natural early-warning system of erosion on open muddy coasts in French Guiana, in: F. Sidik and D. A. Friess (Eds.), Dynamic Sedimentary Environments of Mangrove Coasts, pp. 47-66, https://doi.org/10.1016/B978-0-12-816437-2.00011-2

Reguero B.G., Losada I.J. and Méndez F.J., 2019. A recent increase in global wave power as a consequence of oceanic warming. Nature Communications. 10, 205. http://doi.org/10.1038/s41467-018-08066-0

Robinet A., Idier D., Castelle B. and Marieu V., 2018. A reduced-complexity shoreline change model combining longshore and cross-shore processes: The LX-Shore model. Environmental Modelling & Software. 109, pp. 1-16. https://doi.org/10.1016/j.envsoft.2018.08.010

Rodriguez H.N. and Mehta A.J., 2001. Modeling Muddy Coast Response to Waves. Journal of Coastal Research. pp. 137-148. https://www.jstor.org/stable/25736169

Russeil V., Lo Seen D., Broust F., Bonin M. and Praene J.-P., 2023. Food and electricity self-sufficiency trade-offs in Reunion Island: Modelling land-use change scenarios with stakeholders. Land Use Policy. 132, 106784. https://doi.org/10.1016/j.landusepol.2023.106784

Saenger P., 2003. Mangrove Ecology, Silviculture and Conservation. Kluwer Academic Publishers.

Santos V.F., Short A.D. and Mendes A.C., 2016. Beaches of the Amazon Coast: Amapá and West Pará, in: A. D. Short and A. H. d. F. Klein (Eds.), Brazilian Beach Systems, Coastal Research Library, 67-93, https://doi.org/10.1007/978-3-319-30394-9_3

Seddon N., Smith A., Smith P., Key I., Chausson A., Girardin C., House J., Srivastava S. and Turner B., 2021. Getting the message right on nature-based solutions to climate change. Global Change Biology. 27, pp. 1518-1546. https://doi.org/10.1111/gcb.15513

Splinter K.D. and Coco G., 2021. Challenges and Opportunities in Coastal Shoreline Prediction. Frontiers in Marine Science. 8, 788657. https://doi.org/10.3389/fmars.2021.788657

Tanaka N., Sasaki Y., Mowjood M.I.M., Jinadasa K.B.S.N. and Samang Homchuen S., 2007. Coastal vegetation structures and their functions in tsunami protection: experience of the recent Indian Ocean tsunami. Landscape and Ecological Engineering. 3, 33-45.

Temmerman S., Horstman E.M., Krauss K.W., Mullarney J.C., Pelckmans I. and Schoutens K., 2023. Marshes and Mangroves as Nature-Based Coastal Storm Buffers. Annual Review of Marine Science. 15, pp. 95-118. https://doi.org/10.1146/annurev-marine-040422-092951

Toimil A., Losada I.J., Nicholls R.J., Dalrymple R.A. and Stive M.J.F., 2020. Addressing the challenges of climate change risks and adaptation in coastal areas: A review. Coastal Engineering. 156, 103611. https://doi.org/10.1016/j.coastaleng.2019.103611

Toorman E.A., Anthony E., Augustinus P.G.E.F., Gardel A., Gratiot N., Homenauth O., Huybrechts N., Monbaliu J., Moseley K. and Naipal S., 2018. Interaction of Mangroves, Coastal Hydrodynamics, and Morphodynamics Along the Coastal Fringes of the Guianas, in: C. Makowski and C. W. Finkl (Eds.), Threats to Mangrove Forests: Hazards, Vulnerability, and Management, pp. 429-473, https://doi.org/10.1007/978-3-319-73016-5_20

Tran A., Fall A.G., Biteye B., Ciss M., Gimonneau G., Castets M., Seck M.T. and Chevalier V., 2019. Spatial Modeling of Mosquito Vectors for Rift Valley Fever Virus in Northern Senegal: Integrating Satellite-Derived Meteorological Estimates in Population Dynamics Models. Remote Sensing. 11, 1024. https://doi.org/10.3390/rs11091024

Tucker G.E. and Hancock G.R., 2010. Modelling landscape evolution. Earth Surface Processes and Landforms. 35, pp. 28-50. https://doi.org/10.1002/esp.1952

Valters D., 2016. Modelling Geomorphic Systems: Landscape Evolution, in: S. J. Cook, L. E. Clarke and J. Nield (Eds.), Geomorphological Techniques, Chap. 5, Sec. 6.12, https://doi.org/10.13140/RG.2.1.1970.9047

Walcker R., Anthony E.J., Cassou C., Aller R.C., Gardel A., Proisy C., Martinez J.-M. and Fromard F., 2015. Fluctuations in the extent of mangroves driven by multi-decadal changes in North Atlantic waves. Journal of Biogeography. 42, pp. 2209-2219. https://doi.org/10.1111/jbi.12580

Wang Y., Healy T., Augustinus P., Baba M., Bao C., Flemming B., Fortes M., Han M., Marone E., Mehta A., Ke X., Kirby R., Kjerfve B., Schaeffer-Novelli Y. and Wolanski E., 2002. Chapter Two Definition, properties, and classification of muddy coasts, in: T. Healy, Y. Wang and J.-A. Healy (Eds.), Proceedings in Marine Science, pp. 9-18, https://doi.org/10.1016/S1568-2692(02)80076-6

Winterwerp J.C., Graaff R.F.d., Groeneweg J. and Luijendijk A.P., 2007. Modelling of wave damping at Guyana mud coast. Coastal Engineering. 54, pp. 249-261. https://doi.org/10.1016/j.coastaleng.2006.08.012